THE JOURNAL OF PHYSICAL CHEMISTRY C

Article

pubs.acs.org/JPCC

Nonadiabatic Spin–Orbit Excitation Dynamics in Quantum-State-Resolved NO($^2\Pi_{1/2}$) Scattering at the Gas–Room Temperature Ionic Liquid Interface

Amelia Zutz and David J. Nesbitt*

JILA, University of Colorado and National Institute of Standards and Technology, and Department of Chemistry and Biochemistry, University of Colorado, Boulder, Colorado 80309-0440, United States

ABSTRACT: Room temperature ionic liquids (RTILs) offer an extremely promising new class of solvents with chemical control of bulk gas solubility, but surprisingly little is known about detailed molecular scale interactions at the gas–liquid interface. In this work, quantum state-to-state resolved collision dynamics at the gas–liquid interface are studied by scattering a jet-cooled molecular beam of ground state NO($^2\Pi_{1/2}$; N = 0) molecules from 1-butyl-3-methylimidazolium bis(trifluoromethylsulfonyl)imide (i.e., $[bmim]^+[Tf_2N]^-$) RTIL, with the resulting rovibronic state distributions probed via laser-induced fluorescence as a function of incident collision energy (E_{inc}) and surface temperature (T_s). Significant excitation is observed from ground ($^2\Pi_{1/2}$) to excited ($^2\Pi_{3/2}$) spin–orbit states, highlighting the presence of electronically nonadiabatic effects at the gas–RTIL interface sensitive to both E_{inc} and T_s. At low collision energies (E_{inc} = 2.7(9) kcal/mol), the two spin–orbit manifold rotational distributions are well described by a single temperature, but with (i) $T_{rot}(^2\Pi_{1/2})$ consistently 30 K *lower* than $T_{rot}(^2\Pi_{3/2})$, and (ii) both temperatures lower than T_s. At high collision energies (E_{inc} = 20(6) kcal/mol), the rotational populations are well fit to two-temperature "trapping-desorption" (TD) and "impulsively scattered" (IS) distributions, with the branching ratio into the TD channel (α) for $^2\Pi_{1/2}$ consistently *higher* than that for the spin–orbit excited $^2\Pi_{3/2}$ state. From detailed balance considerations these rotational temperatures, in both the low collision energy and TD component of the high collision energy scattered flux, imply the presence of electronic and rotational state dependent trapping-desorption probabilities and provide new theoretical challenges to high level modeling of collision dynamics at the gas–RTIL interface.

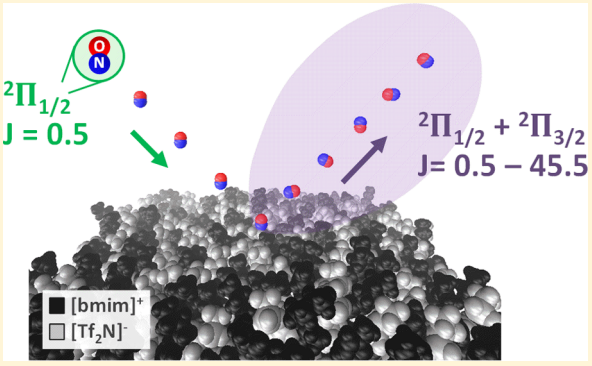

I. INTRODUCTION

The surface of a liquid represents an unusually complex and yet intensely relevant nanoscale environment for chemistry, the further elucidation of which is currently one of the major frontier challenges for the chemical physics community. Detailed molecular energy transfer and molecular dynamics at gas–liquid interfaces are crucial to understanding chemical pathways such as (i) gas adsorption, accommodation, and dissolution into liquids, (ii) reactive processing of atmospheric aerosols, and (iii) heterogeneous gas–liquid catalytic processes.[1−4] Indeed, energy transfer from one molecule to another via inelastic scattering represents a fundamental collisional process that, when coupled with molecular scattering experiments, can yield important insights into both the structure and dynamics of liquid interfaces.[5] The energy transfer between translational, rotational, vibrational, and electronic degrees of freedom of a gas projectile and the liquid surface has been probed with the combination of time-of-flight mass spectrometry and universal detection methods.[6−10] Additional information has been obtained at the quantum state level arising from more recent laser-based techniques such as direct IR absorption, multiphoton ionization/velocity map imaging, and laser-induced fluorescence.[11−18] In close conjunction with molecular dynamics simulations,[6,19−22] these experiments have begun to elucidate probabilities for gas molecules sticking/dissolving/desorbing or directly scattering at liquid surfaces. In particular, the synergism between experimental and theoretical efforts has provided substantial evidence for a simple physical picture of *microscopic branching*, whereby incident gas molecules transfer some of their translational energy and can either (i) transiently trap on the surface, thermalize, and desorb (trapping-desorption, TD) or (ii) scatter more or less directly from the surface without complete loss of initial collision conditions (impulsive scattering, IS).[5,9,14,15,20] Knowledge of such interactions is crucial to developing a better predictive understanding of dynamical processes at gas–liquid interfaces, most notably the kinetics and thermodynamics of adsorption/solvation of gases into the liquid phase.[1,23,24]

To both explore and exploit such fundamental understanding, it is particularly useful to have "tunable" solvent systems for study, such as afforded by room temperature ionic

Received: September 20, 2014
Revised: February 9, 2015
Published: March 24, 2015

DOI: 10.1021/jp509522c
J. Phys. Chem. C 2015, 119, 8596–8607

liquids (RTILs). As the name implies, RTILs represent a novel class of designer solvents that are liquid at room temperature and yet exhibit extremely low vapor pressures due to strong cation/anion Coulomb interactions. These molten ionic salts are versatile, green solvents due to their high solubility, low vapor pressures, and chemical and thermal stability. Most importantly, by changing either the cation or anion structure, or even altering a functional group within an ion, the properties of ionic liquids can be tuned to selectively dissolve specific molecules, with an enormous range of potential applications in electrochemical, biological, analytical, and engineering fields.[25,26] More specifically, RTILs are being developed for use in fuel cells,[27] solar panels,[28] electrolytes in batteries,[29] drug delivery,[30] and a variety of extraction schemes.[31,32] By way of examples, commercial separation of H_2 from CO in steam gas reformation, or CO_2 sequestration from power plants based on differential solubility in RTIL solvents are actively being considered,[32−35] for which a detailed understanding of the gas−RTIL interface would obviously be a crucial first step. One parallel direction of keen interest is the investigation of *open shell*, *radical* systems, which now introduce the role of non-Born−Oppenheimer surface hopping between multiple electronic states as well as differential chemical reactivity and even potential prospects for stereochemical dynamics.[36−39]

In order to explore such issues, we have developed novel capabilities for probing internal rovibronic energy distributions of *open shell* NO molecules scattered at the *gas−ionic liquid* interface. Nitric oxide is an open shell radical with nonzero total angular momentum and multiple low-lying electronic states, which allow the electronic degree of freedom in a gas−liquid molecular scattering experiment to be explored. The scattered molecules are probed with laser-induced fluorescence (LIF) in the ground $X(^2\Pi)$ electronic state, which is composed of spin−orbit ground ($^2\Pi_{1/2}$) and excited ($^2\Pi_{3/2}$) state manifolds separated by a spin−orbit splitting of $E_{SO} \approx 123$ cm^{-1}.[40] For *low* end-over-end tumbling angular momenta (N), energy differences between NO rotational states ($\approx 2B_{NO}N$) are small with respect to E_{SO}. Thus, both electron orbital and spin angular momenta are strongly coupled to the NO internuclear bond (i.e., Hund's case (a)), with the total angular momentum projection along the internuclear axis ($\Omega = 1/2, 3/2$) as a good quantum number. Within each spin−orbit state submanifold, there are also two weakly split Λ-doublet states of opposite overall parity, which semiclassically correspond to the half-filled orbital either parallel (e) or perpendicular (f) to the plane of rotation.[41] Most importantly, all four electronic states for each rovibrational NO(v,J) can be independently detected by UV-laser-induced fluorescence on the $A(^2\Sigma^+) \leftarrow X(^2\Pi)$ band. This permits exploration of surface hopping between these low-lying electronic states arising from collisions at the gas−liquid interface. As will be seen in more detail, this provides an especially interesting molecular probe of electron dynamics during a collisional event, which can be of particular relevance to liquid systems with high charge densities such as surface anions in ionic conductors like RTILs as well as free electron carrier motion in molten metals.[36,37]

Recently, a number of experimental and theoretical studies have explored the gas−RTIL interface, with imidazolium-based ionic liquids being of specific interest due to their wide range of applications.[25,26,33,42] One particular focus of such research efforts has been on microscopic surface composition, specifically the relative abundance of anions and cations at the interface, as well as the placement and orientation of functional groups.[16,17,22,43−46] For example, surface tension measurements[43] as a function of bulk composition provided early insights into the synergism between van der Waals, hydrogen bonding, and electrostatic interactions at the interface. At a more refined molecular level, the surfaces of these liquids have been probed with nonlinear $\chi^{(2)}$ methods such as sum frequency generation spectroscopy (SFG),[43,47,48] which by virtue of phase matching constraints only probes molecules within the first few monolayers of the gas−liquid interface, while rejecting contributions from deeper into the bulk. Similarly, angle-resolved X-ray photoelectron spectroscopy (ARXPS) methods have also been used to explore the composition at the gas−RTIL interface, exploiting angle and kinetic energy resolved escape of electrons into the vacuum from molecules within one electron scattering length from the surface.[44−46,49]

Inelastic[16,18] and reactive[6,12] molecular scattering experiments offer particular advantages in probing only the topmost molecular layer and which therefore have provided valuable data for molecular interactions at the gas−RTIL interface as well as help characterize the composition and orientation of molecules present at the surface. For example, hydrogen abstraction scattering methods (e.g., $O(^3P)$ + liquid surface → $OH(^2\Pi)$ or $F(^2P)$ + liquid surface → HF)[6,12,50] have been especially useful in characterizing the presence of alkyl hydrocarbon species at RTIL surfaces,[2,4,38] while inelastic scattering experiments can explore interfacial properties via composition-dependent energy transfer into internal degrees of freedom of the projectile.[16,18] In conjunction with theoretical calculations,[6,22] such experiments have shown that alkyl chains on imidazolium cations near the surface act quite hydrophobically and preferentially point into the vacuum. Furthermore, theory predicts a significant thermodynamic propensity for bulky anions to preferentially occupy the topmost layer, which therefore compete with larger alkyl chains for surface sites.[22] This naturally leads to a balance in thermodynamic driving forces between anion size and alkyl chain length for the top surface layer, which in turn can control the degree of hydrophobicity in the gas−liquid interfacial region. Indeed, the relative abundances of anions vs cations, as well as different functional groups within each of these ions, clearly must influence the energy transfer and collision dynamics for incident gas molecules striking the RTIL surface.

Of particular interest is the potential role of partial electron transfer between interfacial ions and colliding projectiles at the gas−RTIL interface, which could be especially relevant when considering nonadiabatic surface hopping effects in open-shell NO + RTIL collision dynamics.[36] RTILs comprise a complex liquid mixture of nevertheless strongly interacting ions and as a result exhibit interesting surface electronic properties that can be explored using XPS, ultraviolet photoelectron spectroscopy (UPS), and soft X-ray emission spectroscopy (SXES).[51] Because of finite electron scattering lengths, SXES and UPS are both interfacial region-specific techniques that can probe the valence band of liquids with low vapor pressures, which Kanai et al. have exploited to suggest that the HOMO (highest occupied molecular orbital) state in $[bmim]^+[Tf_2N]^-$ is delocalized over *both cation* and *anion* species.[52] Interestingly, this conclusion was found to be anion dependent over a series of imidazolium-based RTILs. For example, the HOMO and LUMO (lowest unoccupied molecular orbital) states are thought to be localized primarily on the *cation* for $[bmim]^+[BF_4]^-$ and $[bmim]^+[PF_6]^-$ RTILs, but which

DOI: 10.1021/jp509522c
J. Phys. Chem. C 2015, 119, 8596−8607

contrasts with what has been reported for $[bmim]^+Cl^-$ and $[bmim]^+Br^-$ RTILs, where the HOMO is attributed primarily to the *anion*. Indeed, this would also be consistent with typical *inorganic* ionic liquids like molten NaCl, where the top valence band is localized on the Cl^- anion.[53] However, this also invites comparison with bulky anions such as $[TF_2N]^-$, for which molecular orbital calculations on $[bmim]^+[Tf_2N]^-$ suggest that the HOMO is energetically *higher* than the valence band. This can be rationalized on the basis of the Madelung potential for each ion, e.g., energy level shifts due to electrostatic *destabilization* of the $[bmim]^+$ *cation* molecular orbitals by the surrounding RTIL environment, whereas the molecular orbitals of the *anion* become preferentially stabilized.[52,54] This is particularly relevant with open shell radical projectiles like NO, for which nonadiabatic effects can play a large role in gas−liquid collision dynamics, with the further intriguing possibility of transient electron transfer amplitude in the interfacial region.

The present work represents a systematic study of quantum state resolved scattering of NO from the gas−$[bmim]^+[Tf_2N]^-$ RTIL interface. The organization of this paper is as follows. In section II, we provide a brief overview of relevant aspects of the experiment, followed in section III by results and analysis on quantum state resolved final rovibronic distributions as a function of (i) incident collision energy and (ii) RTIL surface temperature. As a key observation, we see evidence for strongly nonequilibrium as well as nonadiabatic dynamics in the scattered flux, both at low (2.7(9) kcal/mol) and hyperthermal (20(6) kcal/mol) collision energies. This is followed in section IV by a discussion of possible origins for such nonthermal, surface hopping phenomena. This is aided by preliminary MOLPRO CCSD(T) and multireference calculations of *ab initio* equilibrium geometries and well depths for the simple model NO + Cl^- collision system, with summary and conclusions presented in section V.

II. EXPERIMENTAL SECTION

A brief description of the experimental setup is described herein, with more thorough descriptions found in previous studies on NO scattering from liquid gallium and imidazolium-based RTILs.[17,18] A collimated molecular beam of NO is directed at a liquid reservoir, and the scattered molecules are detected with rovibrational, electronic spin−orbit, and Λ-doublet state resolution. An illustration of the experimental setup is shown in Figure 1, where the $[bmim]^+[Tf_2N]^-$ liquid surface displayed is based on quantum mechanics/molecular mechanics (QM/MM) molecular dynamics simulations by Schatz et al.[22] The incident molecular beam is supersonically expanded from an Evan−Lavie pulsed valve (100 μm diameter pinhole, 3000 Torr backing pressure, 80 μs pulse width) and is rotationally and electronically cold; all NO molecules are in the ground spin−orbit state ($^2\Pi_{1/2}$), with equal Λ-doublet populations, and a rotational temperature ≈ 1 K (as shown in previous work[17]), corresponding to ∼95% of the NO molecules in the $^2\Pi_{1/2}$, $N = 0$ state. Within the limit of our LIF detection sensitivity (1 part in 10^4), we detect no vibrationally excited NO molecules in the incident beam. The molecular beam is composed of 1% NO/99% buffer gas, using H_2 or Ne-70 (70% Ne, 30% He) in order to vary E_{inc} from 2.7(9) up to 20(6) kcal/mol, respectively, with ≤1% NO in the buffer gas optimized to eliminate dimer formation. The molecular beam passes through a 3 mm skimmer 5.3 cm downstream from the valve orifice and travels another 8.6 cm to the surface, where the collimated beam strikes the surface at a 45° angle on a 0.8 cm × 1.1 cm area spot size. The gas−liquid molecular scattering occurs in a 96 L stainless steel vacuum chamber with a 1500 L/s turbopump, which establishes a base pressure of 2 × 10^{-8} Torr.

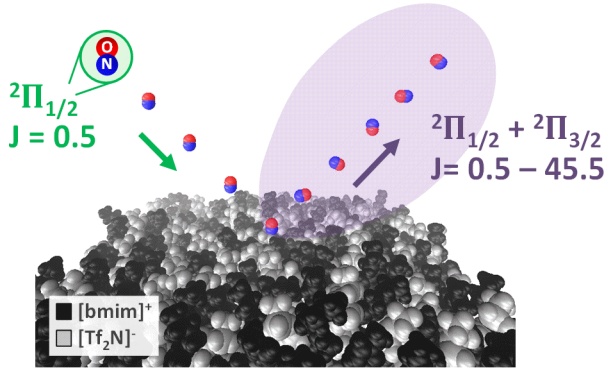

Figure 1. Dynamics at the gas−RTIL interface are probed by directing a molecular beam of supersonically cooled NO at RTIL liquid surfaces and detecting scattered molecules with full quantum state resolution. All incident NO molecules are in the ground spin−orbit state ($^2\Pi_{1/2}$) and are rotationally cooled ($T_{rot} \approx 1$ K), while rotational levels up to $J = 45.5$ for both ground and excited spin−orbit states are detected in the scattered molecules after collisions with the surface. The liquid studied is 1-butyl-3-methylimidazolium bis(trifluoromethylsulfonyl)-imide (i.e., $[bmim]^+[Tf_2N]^-$), where $[bmim]^+$ and $[Tf_2N]^-$ are shown in black and gray, respectively, in the simulated RTIL interface calculated by Schatz et al.[22]

Scattered molecules are state-selectively detected using laser-induced fluorescence (LIF) by electronically exciting NO molecules via the γ-band ($A(^2\Sigma^+) \leftarrow X(^2\Pi)$) with a UV pulsed laser and imaging the fluorescence back down to the $^2\Pi$ ground state on a photomultiplier tube (PMT). A pulsed UV light source is generated by tripling the output of a YAG-pumped-dye laser, operating at 10 Hz with LDS-698 dye. The resulting light is ∼225 nm with 0.4 cm^{-1} line width, with pulse energies ≤5 μJ/pulse to avoid saturation of LIF transitions. The range of laser intensities is confirmed against studies of NO room temperature distributions and further checked for clustering effects by curve of growth measurements. The dye laser is scanned over an 800 cm^{-1} range in order to detect all electronic spin−orbit, Λ-doublet, and rovibrational states ($J \leq 45.5$) significantly populated. The fluorescence signal on a PMT is electronically gated in time and normalized to the laser energy for each pulse. The laser beam runs parallel to the surface (1.6 cm above the surface) and in the plane of specular scattering and is delayed approximately 200 μs (varies with E_{inc}) in time with respect to the gas pulse, which is chosen so that molecules are detected at the peak of the scattered NO signal. A 1:1 confocal lens imaging setup with a 4 mm iris collects the fluorescence for a well-defined volume of scattered molecules (∼15 mm^3), the size of which is determined by the diameter of the iris and the laser beam width/height. The spot size of the incident gas molecules on the surface, along with the LIF detection volume, results in the range of scattered angles detected at $\theta_{scatt} = 45 \pm 10°$, with some preliminary scattering angle studies obtained at normal incidence ($\theta_{scatt} = 0 \pm 12°$). It is worth noting that any such fluorescence detection measures the density rather than the flux of scattered molecules, which therefore proportionally underrepresents flux for species with larger velocity components perpendicular to the laser probe direction.

DOI: 10.1021/jp509522c
J. Phys. Chem. C 2015, 119, 8596−8607

The liquid surface studied herein is $[bmim]^+[Tf_2N]^-$ purchased from Iolitec with 99% purity. The RTIL material was degassed with moderate stirring and heating at ~60 °C for a minimum of 6 h while being pumped on with a liquid nitrogen cold trap to remove trace amounts of gaseous species. The degassed liquid is placed in a stainless steel crucible with a 4.4 × 2.4 × 0.5 cm^3 reservoir. Resistive heaters can heat the crucible to $T_s \leq 900$ K, though for $[bmim]^+[Tf_2N]^-$ the accessible range is limited to $T_s \lesssim 373$ K due to increase in vapor pressure with temperature.[55] Although the bulk of the experiments have been performed for a stationary liquid surface, the results are consistent with data obtained under conditions where the interface is periodically skimmed *in vacuo* every 5 min.

III. RESULTS AND ANALYSIS

A sample spectrum with typical S/N for NO scattered from $[bmim]^+[Tf_2N]^-$ at E_{inc} = 20(6) kcal/mol is shown in Figure 2a. Each spectrum is modeled with a least-squares fit to Gaussian line shapes, and peak populations are determined by integrating over each peak for rotational states up to J = 45.5 for both Λ-doublet states (*e*, *f*) within each of the two spin−orbit states ($^2\Pi_{1/2}$, $^2\Pi_{3/2}$). Since all incident molecules are rotationally cooled into the ground spin−orbit electronic state, the large number of peaks in the spectrum clearly indicates considerable amount of energy transfer taking place with the surface. Sample relative populations as a function of J for each of the electronic states is shown in Figure 2b. Significant differences are observed in the scattered molecules between the two spin−orbit states due to nonadiabatic collision dynamics. By way of contrast, no differences are observed between the two Λ-doublet states within each spin−orbit state, for which we report simple averages unless otherwise stated. Because of possible quantum state dependence in the adsorption behavior, detailed balance considerations yields no *a priori* prediction of the final scattered quantum states. Nevertheless, it is useful for our purposes to construct Boltzmann plots for populations vs (i) rotational state and (ii) incident beam energy.

IIIA. Low E_{inc} Rotational Distributions (E_{inc} = 2.7 kcal/mol). The data at low incident energies (E_{inc} = 2.7(9) kcal/mol) can be quite well described by linear, single temperature Boltzmann plots, consistent with most NO molecules undergoing trapping-desorption events with complete thermal accommodation (i.e., $\alpha \approx 1$). These sample data in Figure 3 have been taken at a surface temperature of T_s = 292 K, with the plots representing each spin−orbit state, $^2\Pi_{1/2}$ and $^2\Pi_{3/2}$, averaged over nearly equally populated Λ-doublet states. Interestingly, despite low enough collision energies for complete thermal accommodation at the RTIL surface, the scattered molecules observed in the $^2\Pi_{1/2}$ and $^2\Pi_{3/2}$ manifolds are in fact not in equilibrium with each other and instead exhibit *lower* ($T_{rot}(^2\Pi_{1/2})$ = 271(8) K) and *higher* ($T_{rot}(^2\Pi_{3/2})$ = 308(8) K) rotational temperatures than T_s. These effects can be explored in more detail by varying the surface temperature, as shown in Figure 4. The measured rotational temperatures do increase linearly with surface temperature with a slope of ≈ 0.5 and thus distinctly different from unity. More quantitatively, the slopes for the two spin−orbit states are equal but maintain a constant vertical difference ($\Delta T \approx 30$ K) as the surface temperature is varied from 292 to 373 K. By detailed balance considerations, this necessarily implies deviations from unity sticking behavior at the gas−liquid interface and suggests a significant angular and/or spin−orbit dependence to the potential surface for adsorption/desorption.[56]

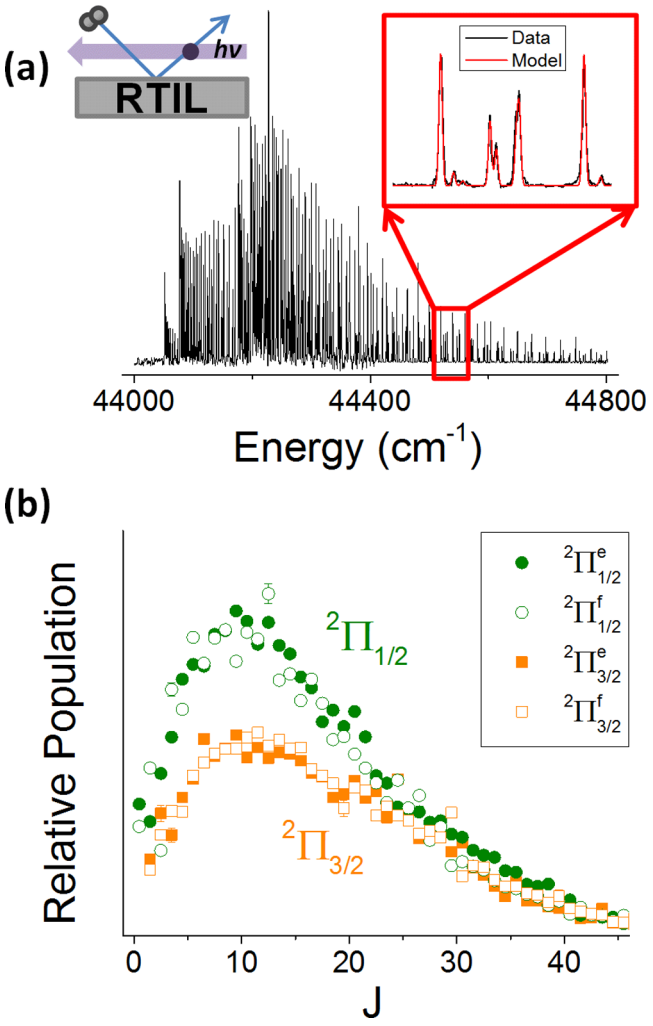

Figure 2. (a) Sample LIF spectrum of scattered NO from $[bmim]^+[Tf_2N]^-$. Each spectrum is fit with a least-squares fit (shown in red in the magnified inset), from which quantum-state resolved populations are extracted. This spectrum is taken at high incident collision energy (E_{inc} = 20 kcal/mol), with T_s = 333 K. As illustrated in the upper left-hand corner, the signal is only measured for a small volume of scattered molecules with $\theta_{scatter}$ = 45 ± 10°. (b) Population distributions corresponding to the above sample spectrum, where the four electronic states ($^2\Pi^e_{1/2}$, $^2\Pi^f_{1/2}$, $^2\Pi^e_{3/2}$, $^2\Pi^f_{3/2}$) are plotted as a function of rotational J state.

These results are surprising and differ qualitatively from previous studies with CO_2 scattering from PFPE at similarly low incident energies (E_{inc} = 1.6 kcal/mol).[14] Specifically, the CO_2 rotational and even translational Doppler line width temperatures in these prior studies were found to be in close agreement with T_s, consistent with the expectation that low-energy incident molecules stick, thermalize, and therefore desorb with quantum state distributions in equilibrium with the surface.[14] However, for open-shell molecules like NO and OH, there is now growing evidence that gas-surface scattering dynamics clearly differ.[57,58] For example, inelastic scattering experiments with NO scattered at low E_{inc} off molten metals and single crystal surfaces yield rotational temperatures with small differences from T_s near room temperature, but which increase significantly as the surface temperature increases, e.g.,

DOI: 10.1021/jp509522c
J. Phys. Chem. C 2015, 119, 8596−8607

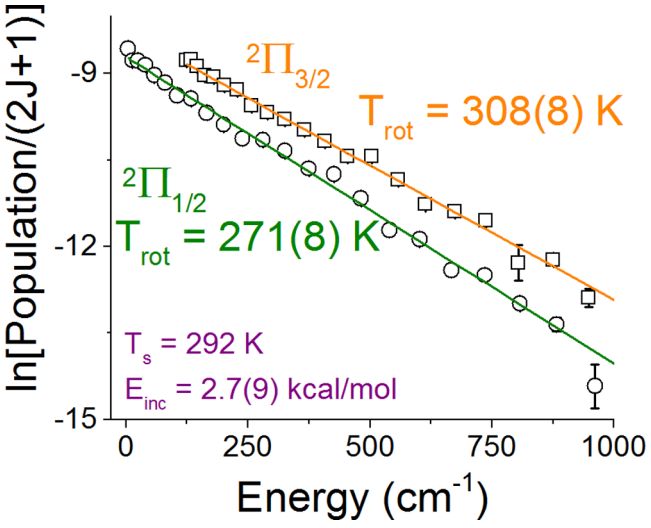

Figure 3. Boltzmann plot of scattered rotational populations at low incident translational energy (E_{inc} = 2.7(9) kcal/mol). These distributions display linear fits to a single temperature distribution, where the Λ-doublet states are experimentally equally populated and therefore averaged for each spin−orbit state. Note that T_s = 292 K and thus that $T_{rot}(^2\Pi_{1/2})$ and $T_{rot}(^2\Pi_{3/2})$ are close to but slightly *cooler* and *hotter* than the liquid interface, respectively.

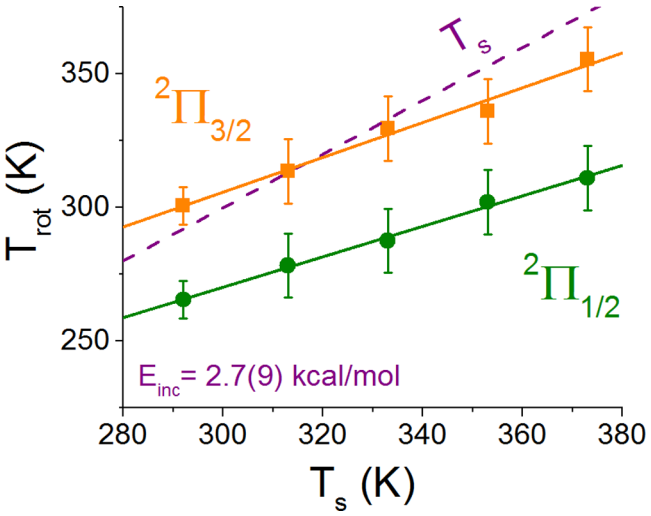

Figure 4. Rotational temperature dependence on T_s for low collision energy (E_{inc} = 2.7(9) kcal/mol). The dotted purple line represents a line of "complete accommodation" or what the rotational distributions would look like if fully equilibrated with the surface temperature (T_s) and the sticking coefficient were unity and independent of rotational state. Note that each spin−orbit state manifold exhibits deviations from but still a sensitivity to T_s. Error bars are based on multiple measurements at each surface temperature.

as much as $\Delta T \approx 300$ K at T_s = 800 K.[57] From an equivalent perspective, temperature-programmed desorption (TPD) experiments have also been conducted on Ru(001) crystals dosed with NO, which from microscopic reversibility samples the quantum state resolved sticking probabilities in the reverse direction.[58] By way of specific example, thermally desorbed NO from Ru(001) is well fit by a single rotational temperature of 235 K, i.e., again significantly *cooler* than the surface temperature of 455 K. Such nonequilibrium dynamics in rotational temperatures between spin−orbit states have also been observed in other $^2\Pi$ projectile scattering experiments. For example, reactive scattering of $O(^3P)$ at squalane liquid surfaces revealed small but statistically significant differences (~20 K) between rotational temperatures for OH product spin−orbit states, with the excited spin−orbit state appearing slightly hotter.[11] Of particular relevance to the present work, studies by Zare et al. on NO scatting from metallic Ag(111) at multiple low collision energies found the excited $^2\Pi_{3/2}$ rotational state manifold to be consistently *hotter* than that of the ground $^2\Pi_{1/2}$ state, yet with both not in equilibrium with the surface temperature.[57,59]

Simple time reversal symmetry and detailed balance ideas[56] can be exploited to provide some insight into the origin of such nonequilibrium dynamics. For a molecular projectile approaching a gas-condensed phase interface in a specific quantum state, incident energy, and angle, there will be a probability to trap long enough to thermalize with the surface and eventually desorb. If this sticking probability is unity for all quantum states, energies, and angles, then, by detailed balance, all molecules that have thermalized on the surface must desorb into a flux weighted equilibrium distribution representative of the surface temperature. This is simply a consequence of the rigorous kinetic constraint, for conditions of a gas in equilibrium with a surface, that the desorbing flux must *maintain* the system in its equilibrium status. Conversely, the *nonequilibrium* distribution of NO observed in the current low-energy scattering experiments necessarily implies that sticking probabilities for the incoming NO molecular beam depend on internal quantum state and/or incident energy.

An even stronger prediction is that detailed balance considerations rigorously require the internal quantum state distributions arising from the surface accommodated fraction (α) for an equilibrium flux of incident molecules at T_s to *exactly* complement those from the nontrapping fraction ($1 - \alpha$) and thereby form a composite distribution in *perfect* equilibrium with the surface temperature. It is important to note that even these low incident energy NO beams are cooled predominantly into the *ground* rotational and spin−orbit state (N = 0, $^2\Pi_{1/2}$) and therefore far from equilibrium with T_s. However, detailed balance requires that the fraction of NO molecules (α) that trap/accommodate with the surface long enough to "forget" this initial condition *must* recapitulate the same distributions (equilibrium or nonequilibrium) as would have been obtained under fully equilibrium incident beam conditions.

Based on the observed NO distributions, these simple but powerful detailed balance ideas make several predictions that stimulate further theoretical exploration. First of all, rotational NO temperatures *lower* than T_s imply that the sticking coefficient (α) must (i) depend on J and (ii) indeed *decrease* with increasing rotational excitation. There are many possible ways to achieve this behavior, e.g., a strong angular dependence on the gas−liquid surface interaction potential. As a result of such angular anisotropy, incoming jet cooled NO can quantum mechanically mix in excited rotations to form states oriented with respect to the surface and thereby achieve a deeper or shallower adsorption well and thus a higher or lower barrier to surface physisorption. A similar argument applies to the spin−orbit state distributions as well, but now with the hotter than T_s rotational temperatures (at T_s = 292 K) for the excited spin−orbit manifold, suggesting a significant shift in the angular anisotropy for the $^2\Pi_{3/2}$ vs $^2\Pi_{1/2}$ NO−RTIL intermolecular potential. Indeed, we have made preliminary steps toward such an analysis with high level *ab initio* calculations, as will be discussed in more detail later in section IV.

DOI: 10.1021/jp509522c
J. Phys. Chem. C 2015, 119, 8596−8607

Finally, we note that the formation of excited spin−orbit states from a purely ground electronic state incident beam requires the presence of *nonadiabatic surface hopping* events between the $^2\Pi_{3/2}$ and $^2\Pi_{1/2}$ manifolds. For the low-energy collisional studies above, this could in principle arise simply from a high probability for trapping-desorption events and therefore sufficient time to equilibrate the spin−orbit degree of freedom with the surface temperature. For example, summed over all rotational states, the relative population ratio between ground and excited spin−orbit states at 292 K is $[^2\Pi_{3/2}]/[^2\Pi_{1/2}] = 0.45(2)$, which is close to but lower than the fully equilibrated T_s predictions of 0.54 (Figure 5). At the highest

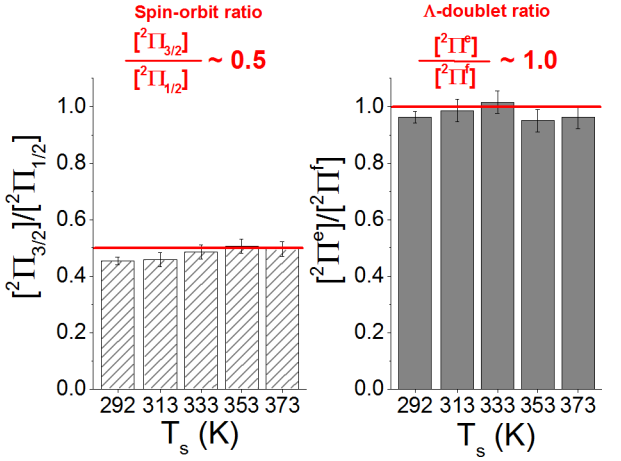

Figure 5. Comparison of electronic state populations relative to each other as the surface temperature is varied for $E_{inc} = 2.7(9)$ kcal/mol. (a) Spin−orbit state ratios, where each spin−orbit state population is summed over all J states and both Λ-doublet states. The spin-orbit ratio $[^2\Pi_{3/2}]/[^2\Pi_{1/2}] \sim 0.45-0.52$ and varies little with T_s. The energy difference between the two spin−orbit state manifolds is 123 cm^{-1}. (b) Λ-doublet electronic ratios are shown on the right, where each Λ-doublet state is summed over all J states and both spin−orbit states. The Λ-doublet states ($\Delta\nu \approx 0.01$ cm^{-1}) are nearly equally populated, independent of surface temperature.

RTIL temperatures sampled ($T_S \approx 373$ K), this spin−orbit population ratio rises to $[^2\Pi_{3/2}]/[^2\Pi_{1/2}] = 0.50(3)$, which is again close to, though still systematically below, the equilibrium value of 0.62. Indeed, much larger deviations from near equilibrium behavior in the spin−orbit distributions are observed at high incident collision energies, as discussed below.

IIIB. High Incident Energy Rotational Distributions (E_{inc} = 20 kcal/mol). With increasing E_{inc}, deviations from this pure trapping desorption behavior due to impulsive scattering events become apparent. In particular, at superthermal collision energies, $E_{inc} = 20(6)$ kcal/mol, there is no longer a linear Boltzmann plot characterized by a single temperature, but instead strong curvature that unambiguously signals the presence of additional *nonequilibuium* rotational dynamics in the scattered flux. As shown in previous work,[8,15,19,23] such distributions can be well fit to a two-temperature model described by eq 1:

$$P_{TD/IS} = \frac{(2J+1)e^{-E_{rot}/kT_{rot}(TD/IS)}}{Q_{rot}(TD/IS)}$$

$$Pop_J = (2J+1)[\alpha P_{TD}(J) + (1-\alpha)P_{IS}(J)] \quad (1)$$

where $\alpha = P_{TD}/(P_{TD} + P_{IS})$ is the branching ratio into the TD channel (with $\alpha = 1$ signaling all molecules undergoing TD scattering) and P_{TD} and P_{IS} represent the respective fractions in the TD and IS component for a given rotational state. Although there must clearly be a continuum of such IS scattering channels, the resulting rotational quantum state distributions are surprisingly well characterized by a "temperature" over 2 orders of magnitude in dynamic range. Such dual temperature behavior has now been verified in many quantum state resolved studies and for many different gas−liquid molecular scatterers as well as confirmed theoretically with detailed trajectory studies.[5,8,12,14,57]

The fundamental source of this rather remarkable simplicity is not yet theoretically well understood; however, we offer the following observations. First of all, there is no *a priori* reason for the nonthermally accommodating IS dynamics to be described by a superthermal Boltzmann distribution; indeed, one would expect deviations from such simple behavior to become evident with sufficient experimental sensitivity. Second, we have recently initiated studies as a function of scattering angle, exploring quantum state resolved NO distributions at both specular ($\theta_{scatt} = 45°$) and normal incidence ($\theta_{scatt} = 0°$). Even for microscopically rough gas−RTIL interfaces, the preliminary results for normal vs specular scattering angles are consistent with the angular trends anticipated for TD vs IS pathways, for example, (i) significant *increase* (20−30%) in fractional trapping-desorption probability α, (ii) significant growth in TD signals with little change in rotational distributions at low E_{inc}, and (iii) significantly *colder* spin−orbit temperatures (T_{elec}). Lastly, such dual temperature Boltzmann behavior necessarily predicts overlapping TD and IS contributions at low final state energies, as clearly verified in the extensive molecular dynamics simulations of Hase and co-workers.[19,20] In any event, such a dual temperature description in eq 1 empirically provides a physically motivated, few parameter characterization of scattered populations over a wide experimental dynamic range (see Figure 6).

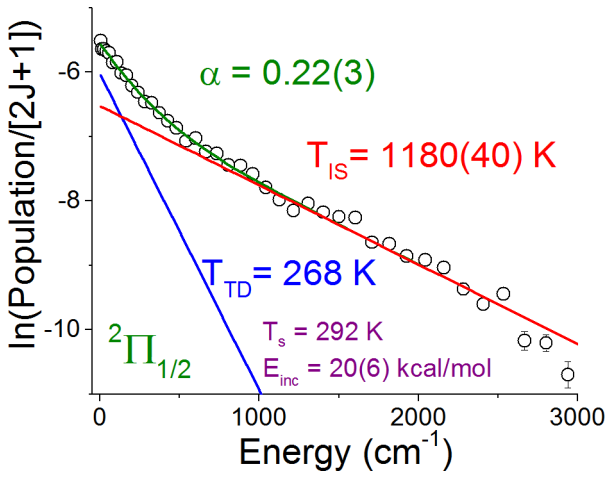

Figure 6. Sample high incident energy ($E_{inc} = 20(6)$ kcal/mol) rotational distributions for the $^2\Pi_{1/2}$ Boltzmann plot. Unlike the *linear trends* exhibited at low E_{inc} (Figure 3), at higher collision energies, distinct *curvature* is observed in the rotational Boltzmann populations. This dynamic range (over 150-fold) is well fit by a dual-temperature distribution, where the lower temperature (T_{TD}) is fixed at values from the low E_{inc} fits, with the hotter temperature (T_{IS}) and branching ratio (α) between to the TD/IS scattering pathways floated.

DOI: 10.1021/jp509522c
J. Phys. Chem. C 2015, 119, 8596−8607

Rotational populations at high collision energies for each spin−orbit state have been fit to eq 1 with α and T_{IS} floated. Consistent with detailed balance considerations, T_{TD} has been fixed at T_{rot} values obtained from the low E_{inc} scattering results for the corresponding surface temperature and spin−orbit state. Figure 6 shows a sample Boltzmann plot for the ground spin−orbit ($^2\Pi_{1/2}$) manifold at E_{inc} = 20(6) kcal/mol; the fitted α and T_{IS} values plotted in Figure 7 as a function of (i) surface temperature and (ii) electronic state, which reveal two significant trends. First of all, the IS temperatures are nearly 3−4-fold hotter than T_s, which indicates the presence of highly rotationally inelastic collisions at superthermal incident energies. Second, the IS temperature component is relatively insensitive to increasing T_s, with the $^2\Pi_{3/2}$ distributions consistently hotter than the $^2\Pi_{1/2}$ state, a pattern also noted above at low E_{inc}. Bimodal rotational distributions have also been observed in orientation-dependent scattering of NO from Ag(111), which have found *hotter* rotational distributions for O-end scattering than for N-end scattering.[60] These effects are most pronounced at more glancing scattering angles (i.e., θ_{scatt} = 70°) and more modest at specular scattering angles. More recent work has been done by Wodtke et al. looking at these orientation effects in scattering vibrationally excited NO from Au (111) and with similar qualitative results.[38,39]

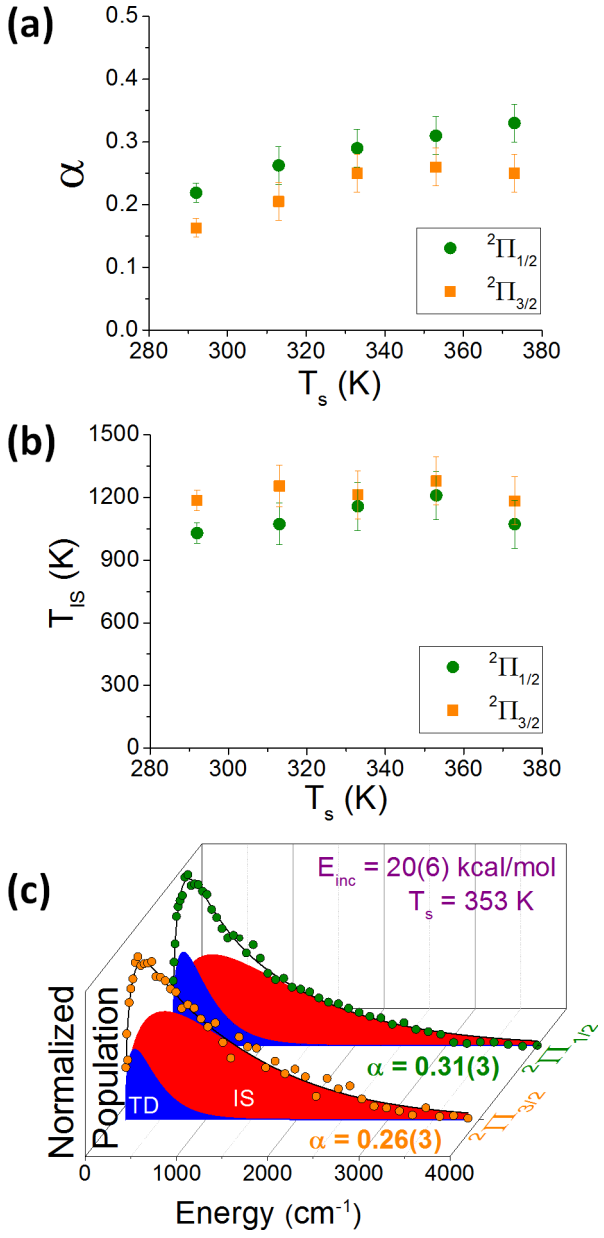

Figure 7. Dependence of T_{IS} and α as a function of surface temperature at E_{inc} = 20(6) kcal/mol. (a) Branching ratios (α) increase systematically with surface temperature, consistent with greater thermal roughening of the RTIL interface. (b) Conversely, T_{IS} is relatively insensitive to surface temperature, with hotter temperatures for $^2\Pi_{3/2}$ vs $^2\Pi_{1/2}$ state manifolds (c) Sample fits to a two temperature distribution for $^2\Pi_{1/2}$ and $^2\Pi_{3/2}$, with total populations normalized to unity. The rotationally cold TD component (blue) represents a significantly larger fraction for $^2\Pi_{1/2}$ vs $^2\Pi_{3/2}$ states, consistent with strong T_s dependent coupling between rotational and spin−orbit degrees of freedom.

It is also worth noting that the branching ratios between the TD and IS channels (α = 0.15−0.30) are surprisingly small at high collision energy, much smaller, for example, than the corresponding values (α = 0.65−0.72) observed for hyperthermal scattering of CO_2 from RTILs.[16] This implies that distributions at these higher incident energies are dominated by nonequilibrium gas−liquid scattering dynamics and indeed, by detailed balance considerations, are consistent with significant deviations from unity sticking behavior also noted in the thermally accommodated flux. There is again a clear spin−orbit state dependence to the accommodation dynamics, with a consistently higher fraction of the spin−orbit conserving collisions ($^2\Pi_{1/2} \rightarrow {}^2\Pi_{1/2}$) proceeding through the TD channel than for the spin−orbit changing events ($^2\Pi_{1/2} \rightarrow {}^2\Pi_{3/2}$). These differences can also be seen directly in the rotational energy distributions in Figure 7c, which reveal a visibly larger fraction of TD collision dynamics in fits for the $^2\Pi_{1/2}$ vs $^2\Pi_{3/2}$ states. The ground electronic state has a higher trapping-desorption component, by roughly 10%, than the excited spin−orbit state. Since all of the incident NO molecules are in the ground spin−orbit state, spin−orbit conserving collisions ($^2\Pi_{1/2} \rightarrow {}^2\Pi_{1/2}$) at 292 K result in thermal accommodation ∼25% of the time, whereas significantly fewer (∼15%) molecules undergoing spin−orbit changing collisions ($^2\Pi_{1/2} \rightarrow {}^2\Pi_{3/2}$) thermalize with the surface. Alternatively stated, the more highly *rotationally inelastic* impulsive scattering (IS) channel appears to be accompanied by a greater propensity for *electronically inelastic* spin−orbit changing collisions. This suggests a strong coupling between rotational and electronic degrees of freedom in the gas−RTIL collision event and offers interesting new challenges to dynamical theory.

It is also worth noting that the fraction of collisions proceeding via the TD pathway increases monotonically with surface temperature. This has been noted previously in other gas−liquid studies[7,8,14] and is consistent with increased inelastic energy loss contributions due to thermally induced surface roughening at higher T_s, thus resulting in a larger fraction of molecules accommodating on the surface. Interestingly, thermal roughening with increased surface temperature does not appear to exert any collateral influence on energy transferred into rotation via the IS channel. Furthermore, despite such strong temperature-dependent effects on the branching ratio α, the corresponding spin−orbit differences are clearly maintained. All of these observations reflect nonunity sticking coefficients and the presence of angular/electronic features in the NO−RTIL potential surface, which translate into a strong sticking

DOI: 10.1021/jp509522c
J. Phys. Chem. C 2015, 119, 8596−8607

dependence on both the incident rotational and spin−orbit state.

IV. DISCUSSION

IVA. Nonadiabatic Electronic Effects. Scattering an open-shell radical species such as NO provides the ability to probe the probability of electronically nonadiabatic events at the gas−liquid interface. In order to explore such surface hopping dynamics in more detail, the rotational populations are summed over all rotational states and are plotted in Figure 5 (E_{inc} = 2.7 kcal/mol) and Figure 8 (E_{inc} = 20 kcal/mol) as a

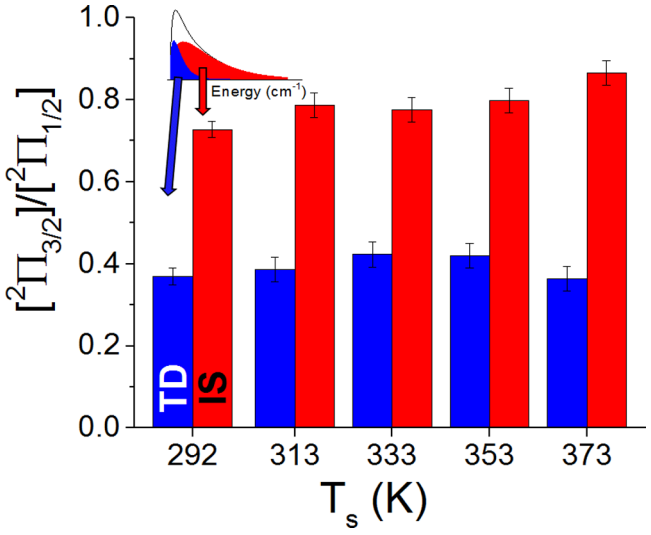

Figure 8. Spin−orbit ratios for the TD and IS scattering channels summed over all rotational and Λ-doublet states for E_{inc} = 20(6) kcal/mol. The ratio of spin−orbit populations within the TD component (blue) is $[^2\Pi_{3/2}]/[^2\Pi_{1/2}] \approx 0.40$, corresponding to an electronic temperature of ∼200 K and relatively insensitive to surface temperature. By way of comparison, the equivalent ratios for the impulsively scattered fraction (red) are $[^2\Pi_{3/2}]/[^2\Pi_{1/2}] \approx 0.70-0.85$, corresponding to a ∼500−1000 K range of electronic temperatures and a gradual increase with T_s.

function of (i) spin−orbit state, (ii) Λ-doublet state (only at low E_{inc}), and (iii) RTIL surface temperature. One message from these plots is unambiguous; since the initial jet cooled beam has a spin−orbit ratio indistinguishable from zero $[^2\Pi_{3/2}]/[^2\Pi_{1/2}] \approx 0.0$, the observation of strong spin−orbit excited populations under both low and high incident collision energy conditions implies the presence of surface hopping effects in the gas-surface collision dynamics. More specifically, Figure 5a reveals that low collision energies achieve spin−orbit population ratios of $[^2\Pi_{3/2}]/[^2\Pi_{1/2}] \approx 0.4-0.5$, with a relatively weak dependence on surface temperature. As noted previously, these values are close to but *consistently lower* than predictions based on complete equilibration with the surface in the desorbing flux, with equivalent electronic spin−orbit temperatures varying between T_{elec} = 215 and 252 K over T_s = 292−373 K. By way of contrast, relative populations for NO molecules scattering into *e* and *f* parity Λ-doublet states are compared in Figure 5b. As also demonstrated in Figure 2, there are no significant differences in the scattered molecules' rotational distributions between the Λ-doublet states within each spin−orbit state, and the ratio of these Λ-doublet states is largely insensitive to changes in the surface temperature.

The nonadiabatic dynamics in the scattered flux are explored further at high collision energies in Figure 8, where the TD and IS contributions are now treated separately, with the spin−orbit ratio within each scattering pathway considered by itself. The TD fraction exhibits a spin−orbit ratio of $[^2\Pi_{3/2}]/[^2\Pi_{1/2}] \sim 0.35-0.40$, with no appreciable dependence on T_s. As expected, these results are quite similar to those previously discussed at low E_{inc}, despite nearly 8-fold higher collision energy. This is consistent with what our fits identify as the TD component, correctly reflecting the fraction of fully thermally accommodated NO trajectories, which from detailed balance considerations must yield the same spin−orbit and Λ-doublet ratios (and indeed rotational distributions) independent of the incident collision energy. By way of contrast, however, this spin−orbit fraction jumps precipitously for the impulsively scattered component, for which there are nearly as many excited as ground spin−orbit state molecules ($[^2\Pi_{3/2}]/[^2\Pi_{1/2}] \sim 0.73-0.85$). Expressed in terms of an equivalent electronic "temperature", this would correspond to a range of T_{elec} from 500 to 1000 K. It is worth noting that this is more consistent with the window of temperatures experimentally observed in the impulsively scattered rotational distributions, which might suggest a simple dynamical picture of coupling/partial equilibration between electronic and rotational degrees of freedom on the time scale of an IS collisional event. Furthermore, there is a clear surface temperature dependence to the nonadiabatic excitation effects in these collisions, with the fraction of excited $^2\Pi_{3/2}$ molecules in the IS channel *increasing* with increasing T_s and ostensibly correlated with microscopic roughening of the RTIL surface. Finally, this trend again highlights the connection between (i) rotationally inelastic and (ii) spin−orbit changing ($^2\Pi_{1/2} \rightarrow {}^2\Pi_{3/2}$) collision dynamics in the impulsive scattering pathway, i.e., that *rotational and electronic* degrees of freedom must be strongly correlated.

IVB. Theoretical Considerations. Though a complete treatment is well beyond the scope of the present work, it is worth briefly exploring the fundamental source of such open-shell nonadiabatic dynamics in NO + RTIL scattering at the gas−liquid interface. To make things simple, we replace the surface by a single scattering center, NO + M, which allows us to borrow directly from the pioneering work of Alexander and co-workers.[61,62] From such studies for NO + rare gas dynamics, this yields A′ and A″ potential surfaces in C_s symmetry, on which the energy transfer collisions occur. As elegantly shown by Alexander and co-workers, *spin−orbit conserving* interactions are governed by the *sum* potential, $V_{sum} = (A' + A'')/2$, while *spin−orbit changing* interactions depend upon the *difference* potential, $V_{diff} = (A'' - A')/2$. V_{diff} provides a description of the electronic anisotropy of the NO molecule as a 2D function of Jacobi coordinates (i) M−N−O bond angle (θ) and (ii) center of mass NO−M separation (R) with respect to the scattering center.[62,63] Far from the scattering center at collinear C_{inv} (M−N−O or M−O−N) geometries, these two adiabatic surfaces are exactly degenerate. However, this degeneracy is broken during approach, the magnitude and geometrical differences of which control the propensity for spin−orbit state changing dynamics.

It is worth stressing that comparably high levels of spin−orbit excitation have been observed in other gas-surface scattering systems, in particular NO + molten gallium[17] and NO + Ag (111).[57] By way of contrast, spin−orbit excitation/deexcitation for crossed molecular beam studies[64] of NO + Ar is diminished by roughly an order of magnitude. This clearly speaks to a

DOI: 10.1021/jp509522c
J. Phys. Chem. C 2015, 119, 8596−8607

Table 1. *Ab Initio* Equilibrium Geometries for X^- + NO, with X^- = Cl^- as a Simple Atomic RTIL Anion[a]

		CCSD(T)				MULTI (2A′ + 2A″) MRCI occ, 15, 4 +Q closed, 9, 1			
basis VnZ-f12	symmetry C_{2v}	$R_{X\text{-}NO}$	θ_{X-NO}	r_{NO}	D_e (kcal)	R_{X-NO}	θ_{X-NO}	r_{NO}	D_e (kcal)
n = 2	A′	4.089	180.0	1.1509	1.22	4.122	180.0	1.1520	1.34
	A′	3.618	101.3	1.1510	1.24	3.690	104.2	1.1520	1.29
	A″	3.165	67.4	1.1571	4.03	3.300	74.3	1.1549	3.56
n = 3	A′	4.098	180.0	1.1499	1.15	4.125	180.0	1.1512	1.25
	A′	3.619	101.2	1.1503	1.21	3.691	104.2	1.1512	1.26
	A″	3.163	67.5	1.1563	4.00	3.301	74.1	1.1541	3.52
CBS	A′	4.098	180.0	1.1500	1.12	4.124	180.0	1.1512	1.22
	A′	3.620	101.1	1.1502	1.18	3.691	104.2	1.1512	1.19
	A″	3.157	67.4	1.1565	3.97	3.302	73.8	1.1542	3.49

[a]Left side: MOLPRO calculations at the CCSD(T)/VnZ-f12 level for n = 2, 3 and extrapolated to the complete basis set (CBS) limit. Right side: multireference MOLPRO calculations (MULTI/MRCI(+Q)) for an explicitly correlated VnZ-f12 basis set (n = 2, 3, and CBS limit). R_{X-NO} and r_{NO} in angstroms, θ_{X-NO} in degrees, D_e in kcal/mol. Note the dramatic difference in equilibrium geometries and well depths for the A′ and A″ potential surfaces, which provides a physical mechanism for the nonadiabatic surface hopping dynamics observed experimentally. See text for details.

significant increase in the V_{diff} potential surface for conducting liquid/single crystal metals and RTILs. As first suggested in vibrational relaxation studies for NO(v) + Au (111) by Tully,[37] Wodtke and co-workers,[65] and later proposed by Alexander et al. for NO + Ag(111),[66] one intriguing reason for such large V_{diff} potential surfaces for conducting liquids and solids could be due to *partial charge transfer* to/from the NO molecule during the collisional process. As discussed previously for imidazolium-based RTILs,[52,54] this could in principle come from either the anion or cation species at the gas−liquid interface, although charge donation from the anion would tend to be more energetically favorable, the simplest of which would be atomic halide anions.

In order to explore the magnitude of such nonadiabatic effects, we have therefore performed preliminary *ab initio* geometry optimizations for the simple model system, NO + Cl^-, using both high level single reference (CCSD(T)) and multireference (CASSCF + MRCI) methods on a MOLPRO software platform. The CCSD(T) calculations have been performed with explicitly correlated f12 electron methods and specially optimized correlation consistent f12 basis sets of Peterson et al. (denoted VnZ-f12, n = 2, 3)[67] and extrapolated to the complete basis set limit (CBS). Each of the equilibrium geometries for A′ and A″ symmetry Cl^-−NO structures at the CCSD(T) level are summarized in the left-hand column of Table 1. Note that the A′ surface exhibits two such weakly bound minima: one for collinear approach with the O end pointing inward toward the Cl^- anion (θ = 180.0°, R = 4.098 Å, r_{NO} = 1.1500 Å, D_e = 1.12 kcal/mol) and a second for a more bent structure (θ = 101.1°, R = 3.620 Å, r_{NO} = 1.1502 Å, D_e = 1.18 kcal/mol), with a very shallow trench and transition state connecting the two equilibrium geometries. Of particular importance, however, there is also a much more strongly bound equilibrium geometry of A″ symmetry, which is bent with the N end pointing preferentially toward the Cl^- anion and far more deeply bound (θ = 67.4°, R = 3.157 Å, r_{NO} = 1.1565 Å, D_e = 3.97 kcal/mol) than either of the two A′ symmetry equilibrium states. This implies a surprisingly large magnitude of the *difference* potential (i.e., V_{diff}) in both well depth and geometry, which from the scattering calculations of Alexander et al. begins to rationalize the high propensity for *spin−orbit state changing* dynamics observed experimentally.

With open-shell radical molecular systems such as NO, it is appropriate to be concerned that single reference *ab initio* quantum calculations, even at the CCSD(T)-f12 level, might prove insufficient for predicting accurate equilibrium geometries and well depths. We therefore have repeated these A′, A″ Cl^-−NO geometry optimizations with multireference MOLPRO methods. Specifically, we start from state-averaged CASSCF (MULTI) calculations with explicitly correlated VnZ-f12 basis sets (n = 2, 3), balanced average over the lowest two A′, A″ states (2A′, 2A″), with (15, 4) and (9, 1) occupied and closed orbitals, respectively. A subsequent multireference calculation with the Davidson correction (MRCI-f12 + Q) is then performed for each of the lowest A′ and A″ symmetry states, with additional reference symmetries specified to ensure balanced configuration spaces for both calculations. When extrapolated to the CBS limit and optimized with respect to all three Jacobi coordinates, the multireference results again reveal the presence of two weakly bound A′ equilibrium structures, one collinear (θ = 180.0°, R = 4.124 Å, r_{NO} = 1.1512 Å, D_e = 1.22 kcal/mol) and one bent structure (θ = 104.2°, R = 3.691 Å, r_{NO} = 1.1512 Å, D_e = 1.19 kcal/mol), with a relatively flat trench connecting the two local minima. Likewise, the mutireference calculations yield a much more strongly bound A″ geometry (θ = 73.8°, R = 3.302 Å, r_{NO} = 1.1542 Å, D_e = 3.49 kcal/mol), in nearly quantitative agreement with CCSD(T) predictions (see Table 1). Once again, it is worth stressing the large shifts in equilibrium geometry and well depth between the A′ and A″ surfaces, which yield both a large difference potential (V_{diff}) and thus provide a clear quantum mechanical mechanism for the strong spin−orbit changing collision dynamics observed experimentally.

As a final comment, it is worth pointing out that the NO bond lengths for both the CCSD(T) and multireference A″ equilibrium geometries are systematically larger (+0.003−0.005 Å) than for either of the corresponding A′ minima. This would suggest a simple physical picture of partial charge donation from the Cl^- anion into the antibonding π^* NO molecular orbitals, as can be confirmed by direct inspection of the wave function composition. Such partial charge transfer mechanisms have been previously invoked to interpret vibrational relaxation and excitation for NO scattering from metals vs insulating systems.[36,68,69] For example, when vibrationally excited NO (v =12) is scattered from *metallic surfaces* with low work functions, the NO molecules readily lose significant amounts of vibrational energy. Electron emission ("chemicurrents") has also been detected from metallic surfaces following collisions with highly vibrationally excited molecules.[69] However, when these same highly vibrationally excited molecules were scattered

DOI: 10.1021/jp509522c
J. Phys. Chem. C 2015, 119, 8596−8607

from *insulating surfaces*, there was only quite modest vibrational relaxation.[68] Such nonadiabatic electronic effects clearly indicate a breakdown of the Born−Oppenheimer approximation, which assumes the electrons can adjust instantaneously to nuclear motion while staying on the same electronic adiabatic potential energy surface. As one simple model of the dynamics, electron−hole pair excitation in metallic surfaces could result in partial electron donation to the incident molecule to form a transient NO^- species, which then flows back into the metallic Fermi sea as the NO scatters away from the surface.

It is therefore of interest whether such a charge transfer picture could also offer a novel mechanism for nonadiabatic NO collision dynamics at the gas−RTIL interface. In particular, charge donation from anions at the gas−liquid interface both into and out of the two π^* antibonding molecular orbitals of NO could facilitate particularly efficient spin−orbit excitation, simply by interchanging the $\Lambda = \pm 1$ projections of the orbital angular momentum and thus achieving the desired change in spin−orbit state ($\Omega = \Lambda + \Sigma$) without any requisite flip of the electron spin projection (Σ). However, additional experimental and theoretical work will clearly be needed to confirm or refute the importance of such a partial charge transfer mechanism in controlling nonadiabatic collision dynamics at the gas−RTIL interface, toward which we hope the present study has provided some stimulation and useful first insights.

V. SUMMARY AND CONCLUSIONS

The gas−RTIL interface has been explored via quantum-state-resolved scattering of supersonically cooled NO molecules from $[bmim]^+[Tf_2N]^-$, where collision dynamics are monitored by observing rovibronic scattered populations as a function of collision energy and surface temperature. By exploiting open-shell NO molecules cooled into the lowest spin−orbit state, "surface hopping" between its multiple low-lying electronic states has been probed, with the presence of strong nonadiabatic collisional processes confirmed via spin−orbit excited molecules in the scattered flux.

At low collision energies (E_{inc} = 2.7(9) kcal/mol), the distribution of scattered NO is well described by a single rotational temperature, however, one that is not in equilibrium with the surface temperature. Furthermore, there is evidence for nonequilibrium *electronic* effects as well; for *spin−orbit changing* collisions ($^2\Pi_{1/2} \rightarrow {}^2\Pi_{3/2}$), T_{rot} is roughly 30 K hotter than for *spin−orbit conserving* collisions with the surface ($^2\Pi_{1/2} \rightarrow {}^2\Pi_{1/2}$). While these collision energies are low enough to facilitate complete accommodation of molecules at the surface, these results clearly indicate (i) a nonunity sticking coefficient as well as (ii) rotational and electronic state dependent sticking probabilities to adsorption/desorption. At higher collision energies (E_{inc} = 20(6) kcal/mol), highly nonequilibrium rotational distributions are observed that can be well fit to a two-temperature distribution, which can be associated with fully accommodated (TD) and all nonaccommodated (IS) scattering pathways. The branching ratio into the TD channel, α, increases with surface temperature, consistent with roughening of the gas−liquid interface. Differences in these branching ratios are also observed between the two spin−orbit state manifolds, which reveal that spin−orbit conserving interactions are correlated more strongly with trapping desorption behavior than the spin−orbit changing collisions. The consistency between such data at both high and low incident collision energies further reinforces the notion that there exist dynamical barriers to adsorption/desorption that are dependent both on spin−orbit electronic state and angular orientation for incident NO molecules striking the RTIL surface.

The propensity for electronic excitation, or nonadiabatic surface hopping, is quantified by summing over all rotational states within each of the electronic states. Negligible differences of the scattered NO molecules are observed between Λ-doublet states, while large differences are seen between the two spin−orbit manifolds. Specifically, at lower collision energies, where the full accommodation pathway is likely to predominate, $[^2\Pi_{3/2}]/[^2\Pi_{1/2}] \sim 0.4$ and is close to thermal equilibrium with the surface temperature. At higher collision energies, conversely, this ratio becomes closer to $[^2\Pi_{3/2}]/[^2\Pi_{1/2}] \sim 0.8$, i.e., substantially higher than predicted from a full equilibration picture. If we consider the TD and IS channels separately, the relative population of the excited spin−orbit state is found to be significantly higher for the IS component, with that pathway therefore being more favorable for electronically inelastic, *spin−orbit changing* collisions.

To explore these nonadiabatic effects further, preliminary *ab initio* calculations for Cl^- + NO, where Cl^- represents a simple RTIL anion, have been performed on a MOLPRO software platform using both single reference CCSD(T) and multi-reference (CASSCF + MRCI) methods. The results predict large differences, in both well depths and equilibrium geometries, between the A′ and A″ potential energy surfaces, which from the work of Alexander and co-workers begins to explain the high propensity for spin−orbit excitation observed experimentally. Additionally the equilibrium bond lengths for the A″ state are found to be systematically longer than the A′ state, consistent with transient partial charge donation from the Cl^- anion into the NO π^* orbital and which raises the possibility of a novel electron exchange mechanism that changes the spin−orbit state. Though there is clearly more work needed to confirm the role of such nonadiabatic pathways, we hope such calculations will serve as motivation for further theoretical efforts exploring the detailed mechanism for spin−orbit excitation at the gas−RTIL interface.

AUTHOR INFORMATION

Corresponding Author

*E-mail djn@jila.colorado.edu; Tel 303-492-8857 (D.J.N.).

Notes

The authors declare no competing financial interest.

ACKNOWLEDGMENTS

This work has been supported by the Air Force Office of Scientific Research (FA9550-12-1-0139), with additional funds for vacuum equipment and lasers provided by the National Science Foundation (CHE1266416, PHYS1125844).

REFERENCES

(1) Davidovits, P.; Kolb, C. E.; Williams, L. R.; Jayne, J. T.; Worsnop, D. R. Mass Accommodation and Chemical Reactions at Gas-Liquid Interfaces. *Chem. Rev.* **2006**, *106*, 1323−1354.

(2) Gertner, B. J.; Hynes, J. T. Molecular Dynamics Simulation of Hydrochloric Acid Ionization at the Surface of Stratospheric Ice. *Science* **1996**, *271*, 1563−1566.

(3) Abbatt, J. P. D. Interactions of Atmospheric Trace Gases with Ice Surfaces: Adsorption and Reaction. *Chem. Rev.* **2003**, *103*, 4783−4800.

(4) Ellison, G. B.; Tuck, A. F.; Vaida, V. Atmospheric Processing of Organic Aerosols. *J. Geophys. Res.: Atmos.* **1999**, *104*, 11633−11641.

DOI: 10.1021/jp509522c
J. Phys. Chem. C 2015, 119, 8596−8607

(5) Saecker, M. E.; Govoni, S. T.; Kowalski, D. V.; King, M. E.; Nathanson, G. M. Molecular-Beam Scattering from Liquid Surfaces. *Science* **1991**, *252*, 1421−1424.
(6) Wu, B. H.; Zhang, J. M.; Minton, T. K.; McKendrick, K. G.; Slattery, J. M.; Yockel, S.; Schatz, G. C. Scattering Dynamics of Hyperthermal Oxygen Atoms on Ionic Liquid Surfaces: [emim][NTf_2] and [C_{12}mim][NTf_2]. *J. Phys. Chem. C* **2010**, *114*, 4015−4027.
(7) King, M. E.; Fiehrer, K. M.; Nathanson, G. M.; Minton, T. K. Effects of Thermal Roughening on the Angular Distributions of Trapping and Scattering in Gas-Liquid Collisions. *J. Phys. Chem. A* **1997**, *101*, 6556−6561.
(8) King, M. E.; Saecker, M. E.; Nathanson, G. M. The Thermal Roughening of Liquid Surfaces and Its Effect on Gas-Liquid Collisions. *J. Chem. Phys.* **1994**, *101*, 2539−2547.
(9) Nathanson, G. M. Molecular Beam Studies of Gas-Liquid Interfaces. *Annu. Rev. Phys. Chem.* **2004**, *55*, 231−255.
(10) Wiens, J. P.; Nathanson, G. M.; Alexander, W. A.; Minton, T. K.; Lakshmi, S.; Schatz, G. C. Collisions of Sodium Atoms with Liquid Glycerol: Insights into Solvation and Ionization. *J. Am. Chem. Soc.* **2014**, *136*, 3065−3074.
(11) Kohler, S. P. K.; Allan, M.; Kelso, H.; Henderson, D. A.; McKendrick, K. G. The Effects of Surface Temperature on the Gas-Liquid Interfacial Reaction Dynamics of O(^{3}P) + Squalane. *J. Chem. Phys.* **2005**, *122*, 24712−24720.
(12) Waring, C.; Bagot, P. A. J.; Slattery, J. M.; Costen, M. L.; McKendrick, K. G. O(^{3}P) Atoms as a Chemical Probe of Surface Ordering in Ionic Liquids. *J. Phys. Chem. A* **2010**, *114*, 4896−4904.
(13) Tesa-Serrate, M. A.; King, K. L.; Paterson, G.; Costen, M. L.; McKendrick, K. G. Site and Bond-Specific Dynamics of Reactions at the Gas-Liquid Interface. *Phys. Chem. Chem. Phys.* **2014**, *16*, 173−183.
(14) Perkins, B. G.; Nesbitt, D. J. Quantum State-Resolved CO_2 Collisions at the Gas-Liquid Interface: Surface Temperature-Dependent Scattering Dynamics. *J. Phys. Chem. B* **2008**, *112*, 507−519.
(15) Perkins, B. G.; Nesbitt, D. J. Quantum-State-Resolved CO_2 Scattering Dynamics at the Gas-Liquid Interface: Incident Collision Energy and Liquid Dependence. *J. Phys. Chem. B* **2006**, *110*, 17126−17137.
(16) Roscioli, J. R.; Nesbitt, D. J. Quantum State Resolved Scattering from Room-Temperature Ionic Liquids: The Role of Cation Versus Anion Structure at the Interface. *J. Phys. Chem. A* **2011**, *115*, 9764−9773.
(17) Ziemkiewicz, M. P.; Roscioli, J. R.; Nesbitt, D. J. State-to-State Dynamics at the Gas-Liquid Metal Interface: Rotationally and Electronically Inelastic Scattering of NO[$^2\Pi_{1/2}$(0.5)] from Molten Gallium. *J. Chem. Phys.* **2011**, *134*, 234703−234714.
(18) Ziemkiewicz, M. P.; Zutz, A.; Nesbitt, D. J. Inelastic Scattering of Radicals at the Gas-Ionic Liquid Interface: Probing Surface Dynamics of Bmim-Cl, Bmim-BF_4, and Bmim-Tf_2N by Rovibronic Scattering of NO $^2\Pi_{1/2}$(0.5). *J. Phys. Chem. C* **2012**, *116*, 14284−14294.
(19) Martinez-Nunez, E.; Rahaman, A.; Hase, W. L. Chemical Dynamics Simulations of CO_2 Scattering Off a Fluorinated Self-Assembled Monolayer Surface. *J. Phys. Chem. C* **2007**, *111*, 354−364.
(20) Nogueira, J. J.; Vazquez, S. A.; Mazyar, O. A.; Hase, W. L.; Perkins, B. G.; Nesbitt, D. J.; Martinez-Nunez, E. Dynamics of CO_2 Scattering Off a Perfluorinated Self-Assembled Monolayer. Influence of the Incident Collision Energy, Mass Effects, and Use of Different Surface Models. *J. Phys. Chem. A* **2009**, *113*, 3850−3865.
(21) Yan, T. Y.; Hase, W. L.; Barker, J. R. Identifying Trapping Desorption in Gas-Surface Scattering. *Chem. Phys. Lett.* **2000**, *329*, 84−91.
(22) Li, X. H.; Schatz, G. C.; Nesbitt, D. J. Anion Effects in the Scattering of CO_2 from the Room-Temperature Ionic Liquids [bmim][BF_4] and [bmim][Tf_2N]: Insights from Quantum Mechanics/Molecular Mechanics Trajectories. *J. Phys. Chem. B* **2012**, *116*, 3587−3602.
(23) Nathanson, G. M.; Davidovits, P.; Worsnop, D. R.; Kolb, C. E. Dynamics and Kinetics at the Gas-Liquid Interface. *J. Phys. Chem.* **1996**, *100*, 13007−13020.
(24) Wilson, M. A.; Pohorille, A. Adsorption and Solvation of Ethanol at the Water Liquid-Vapor Interface: A Molecular Dynamics Study. *J. Phys. Chem. B* **1997**, *101*, 3130−3135.
(25) Plechkova, N. V.; Seddon, K. R. Applications of Ionic Liquids in the Chemical Industry. *Chem. Soc. Rev.* **2008**, *37*, 123−150.
(26) Armand, M.; Endres, F.; MacFarlane, D. R.; Ohno, H.; Scrosati, B. Ionic-Liquid Materials for the Electrochemical Challenges of the Future. *Nat. Mater.* **2009**, *8*, 621−629.
(27) Winther-Jensen, B.; Winther-Jensen, O.; Forsyth, M.; MacFarlane, D. R. High Rates of Oxygen Reduction over a Vapor Phase-Polymerized Pedot Electrode. *Science* **2008**, *321*, 671−674.
(28) Bai, Y.; Cao, Y. M.; Zhang, J.; Wang, M.; Li, R. Z.; Wang, P.; Zakeeruddin, S. M.; Gratzel, M. High-Performance Dye-Sensitized Solar Cells Based on Solvent-Free Electrolytes Produced from Eutectic Melts. *Nat. Mater.* **2008**, *7*, 626−630.
(29) Matsumoto, H.; Sakaebe, H.; Tatsumi, K. Preparation of Room Temperature Ionic Liquids Based on Aliphatic Onium Cations and Asymmetric Amide Anions and Their Electrochemical Properties as a Lithium Battery Electrolyte. *J. Power Sources* **2005**, *146*, 45−50.
(30) Hough, W. L.; Smiglak, M.; Rodriguez, H.; Swatloski, R. P.; Spear, S. K.; Daly, D. T.; Pernak, J.; Grisel, J. E.; Carliss, R. D.; Soutullo, M. D.; et al. The Third Evolution of Ionic Liquids: Active Pharmaceutical Ingredients. *New J. Chem.* **2007**, *31*, 1429−1436.
(31) Huddleston, J. G.; Willauer, H. D.; Swatloski, R. P.; Visser, A. E.; Rogers, R. D. Room Temperature Ionic Liquids as Novel Media for 'Clean' Liquid-Liquid Extraction. *Chem. Commun.* **1998**, 1765−1766.
(32) Blanchard, L. A.; Gu, Z. Y.; Brennecke, J. F. High-Pressure Phase Behavior of Ionic Liquid/CO_2 Systems. *J. Phys. Chem. B* **2001**, *105*, 2437−2444.
(33) Blanchard, L. A.; Hancu, D.; Beckman, E. J.; Brennecke, J. F. Green Processing Using Ionic Liquids and CO_2. *Nature* **1999**, *399*, 28−29.
(34) Kim, Y. S.; Choi, W. Y.; Jang, J. H.; Yoo, K. P.; Lee, C. S. Solubility Measurement and Prediction of Carbon Dioxide in Ionic Liquids. *Fluid Phase Equilib.* **2005**, *228*, 439−445.
(35) Anthony, J. L.; Maginn, E. J.; Brennecke, J. F. Solubilities and Thermodynamic Properties of Gases in the Ionic Liquid 1-n-Butyl-3-Methylimidazolium Hexafluorophosphate. *J. Phys. Chem. B* **2002**, *106*, 7315−7320.
(36) Shenvi, N.; Roy, S.; Tully, J. C. Nonadiabatic Dynamics at Metal Surfaces: Independent-Electron Surface Hopping. *J. Chem. Phys.* **2009**, *130*, 174107−174118.
(37) Shenvi, N.; Roy, S.; Tully, J. C. Dynamical Steering and Electronic Excitation in NO Scattering from a Gold Surface. *Science* **2009**, *326*, 829−832.
(38) Bartels, N.; Golibrzuch, K.; Bartels, C.; Chen, L.; Auerbach, D. J.; Wodtke, A. M.; Schafer, T. Dynamical Steering in an Electron Transfer Surface Reaction: Oriented NO(v = 3, 0.08 < E_i < 0.89 eV) Relaxation in Collisions with a Au(111) Surface. *J. Chem. Phys.* **2014**, *140*, 054710−054718.
(39) Bartels, N.; Golibrzuch, K.; Bartels, C.; Chen, L.; Auerbach, D. J.; Wodtke, A. M.; Schafer, T. Observation of Orientation-Dependent Electron Transfer in Molecule-Surface Collisions. *Proc. Natl. Acad. Sci. U. S. A.* **2013**, *110*, 17738−17743.
(40) Herzberg, G. *Spectra and Molecular-Structure. 1. Spectra of Diatomic-Molecules*; Princeton University Press: Princeton, NJ, 1968.
(41) Alexander, M. H.; Andresen, P.; Bacis, R.; Bersohn, R.; Comes, F. J.; Dagdigian, P. J.; Dixon, R. N.; Field, R. W.; Flynn, G. W.; Gericke, K. H.; et al. A Nomenclature for Lambda-Doublet Levels in Rotating Linear-Molecules. *J. Chem. Phys.* **1988**, *89*, 1749−1753.
(42) Welton, T. Room-Temperature Ionic Liquids. Solvents for Synthesis and Catalysis. *Chem. Rev.* **1999**, *99*, 2071−2083.
(43) Martinez, I. S.; Baldelli, S. On the Arrangement of Ions in Imidazolium-Based Room Temperature Ionic Liquids at the Gas-Liquid Interface, Using Sum Frequency Generation, Surface Potential, and Surface Tension Measurements. *J. Phys. Chem. C* **2010**, *114*, 11564−11575.
(44) Kolbeck, C.; Cremer, T.; Lovelock, K. R. J.; Paape, N.; Schulz, P. S.; Wasserscheid, P.; Maier, F.; Steinruck, H. P. Influence of Different

DOI: 10.1021/jp509522c
J. Phys. Chem. C 2015, 119, 8596−8607

Anions on the Surface Composition of Ionic Liquids Studied Using ARXPS. *J. Phys. Chem. B* **2009**, *113*, 8682−8688.
(45) Lovelock, K. R. J.; Kolbeck, C.; Cremer, T.; Paape, N.; Schulz, P. S.; Wasserscheid, P.; Maier, F.; Steinruck, H. P. Influence of Different Substituents on the Surface Composition of Ionic Liquids Studied Using ARXPS. *J. Phys. Chem. B* **2009**, *113*, 2854−2864.
(46) Hammer, T.; Reichelt, M.; Morgner, H. Influence of the Aliphatic Chain Length of Imidazolium Based Ionic Liquids on the Surface Structure. *Phys. Chem. Chem. Phys.* **2010**, *12*, 11070−11080.
(47) Rivera-Rubero, S.; Baldelli, S. Surface Characterization of 1-Butyl-3-Methylimidazollum Br^-, I^-, PF_6^-, BF_4^-, $(CF_3SO_2)_2N^-$, SCN^-, $CH_3SO_3^-$, $CH_3SO_4^-$, and $(CN)_2N^-$ Ionic Liquids by Sum Frequency Generation. *J. Phys. Chem. B* **2006**, *110*, 4756−4765.
(48) Iimori, T.; Iwahashi, T.; Kanai, K.; Seki, K.; Sung, J. H.; Kim, D.; Hamaguchi, H. O.; Ouchi, Y. Local Structure at the Air/Liquid Interface of Room-Temperature Ionic Liquids Probed by Infrared-Visible Sum Frequency Generation Vibrational Spectroscopy: 1-Alkyl-3-Methylimidazolium Tetrafluoroborates. *J. Phys. Chem. B* **2007**, *111*, 4860−4866.
(49) Lockett, V.; Sedev, R.; Bassell, C.; Ralston, J. Angle-Resolved X-Ray Photoelectron Spectroscopy of the Surface of Imidazolium Ionic Liquids. *Phys. Chem. Chem. Phys.* **2008**, *10*, 1330−1335.
(50) Zolot, A. M.; Dagdigian, P. J.; Nesbitt, D. J. Quantum-State Resolved Reactive Scattering at the Gas-Liquid Interface: F + Squalane ($C_{30}H_{62}$) Dynamics Via High-Resolution Infrared Absorption of Nascent HF(v,J). *J. Chem. Phys.* **2008**, *129*, 194705−194715.
(51) Lovelock, K. R. J.; Villar-Garcia, I. J.; Maier, F.; Steinruck, H. P.; Licence, P. Photoelectron Spectroscopy of Ionic Liquid-Based Interfaces. *Chem. Rev.* **2010**, *110*, 5158−5190.
(52) Kanai, K.; Nishi, T.; Iwahashi, T.; Ouchi, Y.; Seki, K.; Harada, Y.; Shin, S. Electronic Structures of Imidazolium-Based Ionic Liquids. *J. Electron Spectrosc.* **2009**, *174*, 110−115.
(53) Poole, R. T.; Jenkin, J. G.; Liesegang, J.; Leckey, R. C. G. Electronic Band-Structure of Alkali-Halides. 1. Experimental Parameters. *Phys. Rev. B* **1975**, *11*, 5179−5189.
(54) Yoshimura, D.; Yokoyama, T.; Nishi, T.; Ishii, H.; Ozawa, R.; Hamaguchi, H.; Seki, K. Electronic Structure of Ionic Liquids at the Surface Studied by UV Photoemission. *J. Electron Spectrosc.* **2005**, *144*, 319−322.
(55) Zaitsau, D. H.; Kabo, G. J.; Strechan, A. A.; Paulechka, Y. U.; Tschersich, A.; Verevkin, S. P.; Heintz, A. Experimental Vapor Pressures of 1-Alkyl-3-Methylimidazolium Bis-(Trifluoromethylsulfonyl) Imides and a Correlation Scheme for Estimation of Vaporization Enthalpies of Ionic Liquids. *J. Phys. Chem. A* **2006**, *110*, 7303−7306.
(56) Tully, J. C. The Dynamics of Adsorption and Desorption. *Surf. Sci.* **1994**, *299*, 667−677.
(57) Kubiak, G. D.; Hurst, J. E.; Rennagel, H. G.; McClelland, G. M.; Zare, R. N. Direct Inelastic-Scattering of Nitric-Oxide from Clean Ag(111) - Rotational and Fine-Structure Distributions. *J. Chem. Phys.* **1983**, *79*, 5163−5178.
(58) Cavanagh, R. R.; King, D. S. Rotational-State and Spin-State Distributions - NO Thermally Desorbed from Ru(001). *Phys. Rev. Lett.* **1981**, *47*, 1829−1832.
(59) Mcclelland, G. M.; Kubiak, G. D.; Rennagel, H. G.; Zare, R. N. Determination of Internal-State Distributions of Surface Scattered Molecules - Incomplete Rotational Accommodation of NO on Ag(111). *Phys. Rev. Lett.* **1981**, *46*, 831−834.
(60) Geuzebroek, F. H.; Wiskerke, A. E.; Tenner, M. G.; Kleyn, A. W.; Stolte, S.; Namiki, A. Rotational-Excitation of Oriented Molecules as a Probe of Molecule Surface Interaction. *J. Phys. Chem.* **1991**, *95*, 8409−8421.
(61) Alexander, M. H. A New, Fully Ab Initio Investigation of the NO($X^2\Pi$)Ar System. I. Potential Energy Surfaces and Inelastic Scattering. *J. Chem. Phys.* **1999**, *111*, 7426−7434.
(62) Alexander, M. H. Differential and Integral Cross-Sections for the Inelastic-Scattering of NO($X^2\Pi$) by Ar Based on a New Ab-Initio Potential-Energy Surface. *J. Chem. Phys.* **1993**, *99*, 7725−7738.
(63) Smedley, J. E.; Corey, G. C.; Alexander, M. H. Quantum Close-Coupled Studies of Collisions of NO($X^2\Pi$) with a Ag(111) Surface. *J. Chem. Phys.* **1987**, *87*, 3218−3231.
(64) Eyles, C. J.; Brouard, M.; Yang, C. H.; Klos, J.; Aoiz, F. J.; Gijsbertsen, A.; Wiskerke, A. E.; Stolte, S. Interference Structures in the Differential Cross-Sections for Inelastic Scattering of NO by Ar. *Nat. Chem.* **2011**, *3*, 597−602.
(65) Huang, Y.; Wodtke, A. M.; Hou, H.; Rettner, C. T.; Auerbach, D. J. Observation of Vibrational Excitation and Deexcitation for NO(v = 2) Scattering from Au(111): Evidence for Electron-Hole-Pair Mediated Energy Transfer. *Phys. Rev. Lett.* **2000**, *84*, 2985−2988.
(66) Gregurick, S.; Alexander, M. H.; Depristo, A. E. Quantum Scattering Studies of Vibrational-Excitation in Collisions of NO($X^2\Pi$) with a Ag(111) Surface. *J. Chem. Phys.* **1994**, *100*, 610−621.
(67) Vieceli, J. S.; Tobias, D. J. Mass Accomodation Coefficient for Water Vapor on Liquid Water from Computer Simulations. *Abstr. Pap. Am. Chem. Soc.* **2004**, *227*, U1003−U1003.
(68) Wodtke, A. M.; Matsiev, D.; Auerbach, D. J. Energy Transfer and Chemical Dynamics at Solid Surfaces: The Special Role of Charge Transfer. *Prog. Surf. Sci.* **2008**, *83*, 167−214.
(69) White, J. D.; Chen, J.; Matsiev, D.; Auerbach, D. J.; Wodtke, A. M. Conversion of Large-Amplitude Vibration to Electron Excitation at a Metal Surface. *Nature* **2005**, *433*, 503−505.

DOI: 10.1021/jp509522c
J. Phys. Chem. C 2015, 119, 8596−8607